




## $\gamma$ -Ray detection with CsI(Tl) scintillators of the FARCOS array

Elena Geraci<sup>1,2,a</sup> , Giuseppe Cardella<sup>1</sup>, Concettina Maiolino<sup>3</sup>, Nunzia S. Martorana<sup>1</sup>, Luis Acosta<sup>7</sup>, Enrico De Filippo<sup>1</sup>, Filippo Fichera<sup>1</sup>, Brunilde Gnoffo<sup>1,2</sup>, Antonio Grimaldi<sup>1</sup>, Chiara Guazzoni<sup>4,5</sup>, Francesco Librizzi<sup>1</sup>, Francesco Noto<sup>3</sup>, Angelo Pagano<sup>1</sup>, Emanuele V. Pagano<sup>3</sup>, Giuseppe Passaro<sup>3</sup>, Sara Pirrone<sup>1</sup>, Giuseppe Politi<sup>1,2</sup>, Fabio Risitano<sup>1,6</sup>, Francesca Rizzo<sup>2,3</sup>, Paolo Russotto<sup>3</sup>, Gaspare Saccà<sup>1</sup>, Gianluca Santagati<sup>1</sup>, Marina Trimarchi<sup>1,6</sup>, Cristina Zagami<sup>2,3,8</sup>

<sup>1</sup> Dipartimento di Fisica e Astronomia “Ettore Majorana”, Università di Catania, Catania, Italy

<sup>2</sup> INFN Sezione di Catania, Catania, Italy

<sup>3</sup> Laboratori Nazionali del Sud, INFN, Catania, Italy

<sup>4</sup> DEIB, Politecnico di Milano, Milan, Italy

<sup>5</sup> INFN Sezione di Milano, Milan, Italy

<sup>6</sup> Dipartimento di Scienze MIFT, Università di Messina, Messina, Italy

<sup>7</sup> Instituto de Física, Universidad Nacional Autónoma de México, Mexico City, Mexico

<sup>8</sup> Centro Siciliano di Fisica Nucleare e Struttura della Materia, Catania, Italy

Received: 25 July 2023 / Accepted: 28 October 2023

© The Author(s) 2023

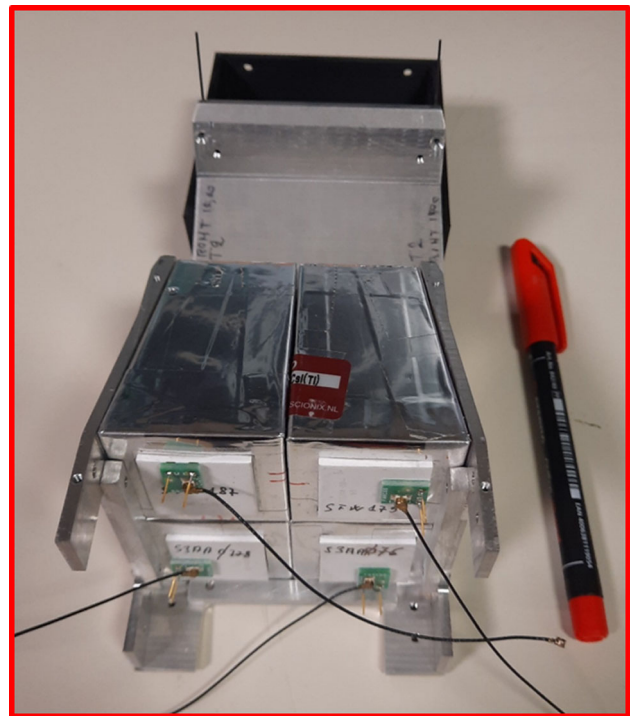
**Abstract** The measurement of the response function of the CsI(Tl) scintillators of the FARCOS array, to standard sources, cosmic rays and environmental background allows the assessment of their performance. Fast–Slow analysis discriminates between  $\gamma$ -rays and charged particles. The relatively good energy resolution allows the observation of well resolved escape peaks due to the interaction of the 4.44 MeV  $\gamma$ -ray generated by AmBe source. Furthermore, the small noise enables to discriminate from the background the annihilation 511 keV  $\gamma$ -rays of the <sup>22</sup>Na source. The energy loss of muons generated by cosmic rays has been also measured and the radioactive contaminants as <sup>137</sup>Cs, <sup>40</sup>K and <sup>208</sup>Tl have been identified. The quality of the detectors suggests the possibility to use the array also for the measurement of  $\gamma$ -ray decay in reactions induced by stable and radioactive beams, once a well-defined reaction channel has been identified. Moreover, a dedicated compact detection module as a portable, high efficiency radiation detector for the control of environmental contamination will be developed.

### 1 Introduction

Cesium iodide detectors are very versatile, relatively low-cost scintillators, widely used in nuclear physics to obtain thick calorimeters able to stop fast charged particles [1–3]. The pure scintillator is a quite fast, radiation and mechanical hard detector [4, 5]. Adding Thallium as doping agent, on the one hand slows the scintillation mechanism, on the other hand enables the charge and mass identification of the detected particles via the well known Fast Slow identification technique as [6–11]. Indeed, the relative contribution of the two components of the light emission in the crystal changes depending on whether  $\gamma$ -rays or charged particles are detected. Many detector arrays were built exploiting this possibility, and various techniques were developed to identify charged particles with different electronic chains [8, 12–14]. A new array named FARCOS (Femtoscope ARray for CORrelations and Spectroscopy) [15, 16] has been recently built with the main purpose to perform particle–particle correlation measurements. The FARCOS array consists of 20 telescopes, each of them made of two stages of Double-Sided Silicon Strip Detectors (DSSSD), with  $32 \times 32$  strips, 2 mm pitch, covering a  $64 \text{ mm} \times 64 \text{ mm}$  active area, and features an angular resolution in the detection of charged particles of about  $0.1^\circ/\text{pixel}$  when placed at 1 m from the target. The telescopes are completed by four CsI(Tl) crystals, with a  $32 \times 32 \text{ mm}^2$  front surface and a length of 60 mm, needed to totally stop high energy particles. The identification capabilities of the CsI(Tl) scintillators are well suited to discriminate in mass and charge particles up to  $Z = 4 - 5$  and  $\gamma$ -rays. In this paper, the merit of the FARCOS CsI(Tl) in the detection of low energy  $\gamma$ -rays (below 10 MeV) has been probed with a good energy resolution suitable to highlight the presence of radioactive contaminants in the environment. This result is achieved even though the dynamics of the used front end electronics was designed for the detection of high energy particles (100 MeV Silicon-equivalent). The measured detector performances are relevant to experiments both in applied and nuclear physics. Following the excellent results shown in this paper, the design of a compact modular and simplified version of the calorimetric stage of the FARCOS detector, as an efficient low-cost radiation monitor for environmental studies, is ongoing. The complete array can be used in order to perform complementary studies on the  $\gamma$ -ray decay of excited nuclei produced in reactions with stable and radioactive ion beams, allowing the extraction

<sup>a</sup> e-mail: [elena.geraci@ct.infn.it](mailto:elena.geraci@ct.infn.it) (corresponding author)

**Fig. 1** Picture of the four CsI(Tl) detectors mounted in a FARCOS telescope main frame, opened on one side. The photodiodes, the connector printed board soldered to them and the small coaxial cables used to connect the preamplifiers can be observed on the backward side of the detectors



of complete spectroscopic information. Section 2 provides description of the setup with particular emphasis on the detector and the related electronics. Section 3 describes the processing techniques used for the acquired data. Section 4 presents the results of the measurement campaign with different radioactive sources and Sect. 5 with cosmic rays and natural background. Section 6 ends with the conclusions and outlook.

## 2 Detectors and electronics description

The FARCOS array [15] is constituted by 20 three stages telescopes. The first two stages are DSSSD detectors, respectively 300  $\mu\text{m}$  and 1500  $\mu\text{m}$  thick. The third stage is constituted by four CsI(Tl) scintillators, of truncated pyramid shape,  $32 \times 32 \text{ mm}^2$  front surface,  $39.5 \times 39.5 \text{ mm}^2$  back surface, 60 mm length with photodiode readout. The photodiodes (Hamamatsu model S-3204-08) have a surface of  $18 \times 18 \text{ mm}^2$  and they are located on the CsI(Tl) back surface. A more complete description of the performance of the array can be found in Ref. [16]. The work reported in this paper focuses only on the CsI(Tl) stage. Figure 1 shows a photograph of four scintillators mounted in the aluminium cage of the telescope. To minimize the stray capacitance, due to interconnection, and so optimizing the noise performance, an ultra-small connector of the serie UFL Hirose was soldered to photodiodes, and short coaxial cables of the same series connect the detectors to the FARCOS front-end motherboard. Each FARCOS front-end motherboard includes two FARCOS ASICs, featuring 16 channels in charge preamplifier configuration for the readout of the DSSSD and one channel also in charge preamplifier configuration with 100 MeV Silicon equivalent full scale energy range [17], for the readout of the photodiode coupled with the CsI(Tl) scintillator. A fully differential line driver drives the signal coming from the charge preamplifier to the outer world through a Samtec twinax edge card cable assembly (ECDP-08-190.0-L1-L2-1-3), collecting the signals of the four scintillators of one telescope and four calibration signals. Signals are digitized by using the GET (Generic Electronics for TPC) electronics [18] at 50 MHz sampling frequency, enough to determine the maximum of the waveform pulse even for the rather slow signals originating from a  $\gamma$ -ray interaction in the scintillator crystal (risetime  $> 2\mu\text{s}$ ). Signals are filtered with a 1  $\mu\text{s}$  Sallen & Key filter to reduce the noise. Since the GET electronics is designed for single ended signals, a custom differential-to-single end converter has been interposed. This converter is mounted on a dual gain programmable module (DGCT), designed by the electronic service of the INFN Sezione di Catania. The DGCT module adds an offset to the signal as needed by the GET electronics. Moreover, it splits the signal into two channels with selectable attenuation or gain factors from 1/16 to 8 in order to fully exploit the available dynamic range. In the case of the  $\gamma$ -rays measurements presented in this paper, a gain equal to 8 has been used, in order to set the full scale energy range to about 12.5 MeV silicon equivalent.

**Fig. 2** Energy spectrum measured with Am-Be source analysed by using different filters. **a** 11 nodes filter, **b** 81 nodes filter, **c** 121 nodes filter, **d** 251 nodes filter. The red curve shown in panels a and b is a Gaussian fit of the first escape peak

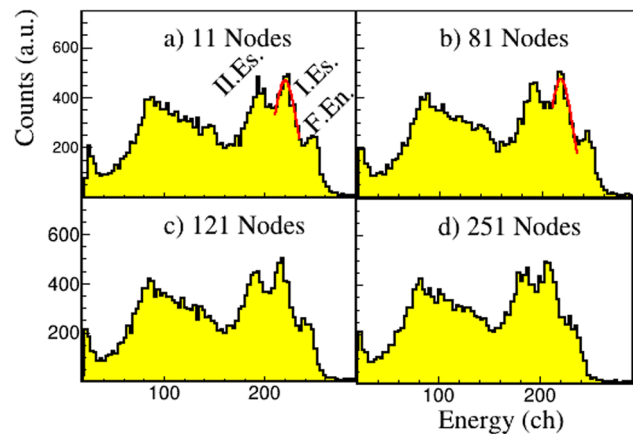
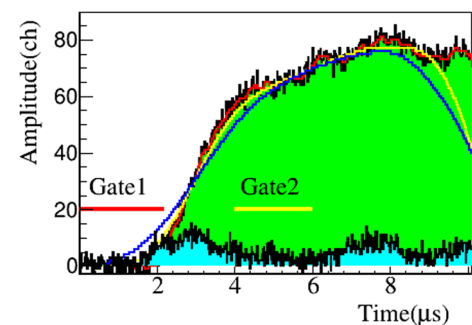


**Fig. 3** Output waveform in the case of the detection of a 1.27 MeV  $\gamma$ -ray (filled green histogram) after FPN subtraction and baseline restoring. The red, yellow and blue lines show the filtered output waveforms after triangular filtering with 11, 81 and 251 nodes respectively. The lines Gate1 and Gate2 indicate the position of the two gates used to evaluate the noise difference integral, see text. The cyan spectrum is a typical noise signal



### 3 Digital signal processing and conditioning of the acquired waveforms

The digitization of the detected signals opens the way to digital signal processing and conditioning in order to better extract the conveyed information in comparison to a standard analogue electronics. In order to estimate the maximum value of the output waveform, proportional to the collected energy, the measured and averaged signal baseline is subtracted on an event by event basis; the noise generated inside the GET electronics, due to the switched capacitors array, is measured in some dedicated channels (called FPN—Fixed Pattern Noise—channels [18]) not connected to any detectors and then subtracted from the original signal. Signal waveforms are then filtered with a triangular filter (11 to 251 nodes—number of channels used by the filter) to improve the signal to noise ratio [19]. As the dominant noise component is the white series noise, for signals generated by direct conversion in silicon detectors, the best energy resolution is obtained using relatively long filters of the order of 151 nodes or more [20]. Instead, due to reasons that will be better shown later, in the case of CsI(Tl) detectors, a smaller number of nodes gives the best noise suppression. Figure 2 shows the energy spectrum obtained with an AmBe  $\gamma$ -ray source by using four different filters with 11, 81, 121, 251 nodes, respectively plotted in panels a, b, c, d. The AmBe source emits neutrons up to  $\approx 10$  MeV, detected with low efficiency in the scintillator, and 4.44 MeV  $\gamma$ -ray originating from the reaction  ${}^9\text{Be} + \alpha \rightarrow n + {}^{12}\text{C}^* + Q$  (5.704 MeV). The 4.44 MeV  $\gamma$ -ray is detected in the scintillator mainly by pair creation. Due to the small size of the scintillator, one or both of the two 511 keV  $\gamma$ -rays produced by the annihilation of the  $e^+$  can escape, giving rise to two escape peaks, well visible in Fig. 2. The full energy peak is less visible, as less probable. As can be observed in Fig. 2, the best energy resolution is obtained by using the filter with 81 nodes, even if the difference with other node numbers is inside the uncertainty. Consequently, the full energy peak can be better appreciated when relatively small values of filter nodes are used, while it tends to disappear with the highest node numbers of the filter (251). It should be emphasized that 512 samples at 50 MHz sampling rate allow to cover up to 10  $\mu\text{s}$  of the output waveform. Therefore, when dealing with the scintillation signal—owing to the slow time constant of the CsI(Tl) in the case of  $\gamma$ -ray interaction—this time window is just enough to observe the maximum of the output waveform and, consequently, in case of filters with high number of nodes some signal loss occurs. Averaging the points with a larger number of nodes causes a decrease of the maximum value of the filtered signal, missing the real one and consequently worsening the signal-to-noise ratio, as clearly shown in Fig. 2. This effect can be better understood by looking at one typical  $\gamma$ -ray waveform. Figure 3 shows the 1.27 MeV  $\gamma$ -ray waveform from  ${}^{22}\text{Na}$  source after baseline restoration and FPN subtraction and, superimposed, the same signal after the filtering with 11 (red), 81 (yellow) and 251 (blue) nodes. While the filter with 11 nodes cannot smooth the relatively low frequency noise, this is instead well suppressed by using 81 nodes. A filter with larger number of nodes, i.e. 251 as the case of the waveform in blue line in Fig. 3, underestimates the real value of the maximum.

**Fig. 4** Noise evaluated as difference between the average value of the signal in the baseline window and around the middle of the time range of the signal

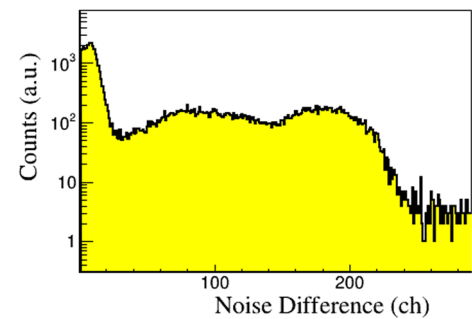
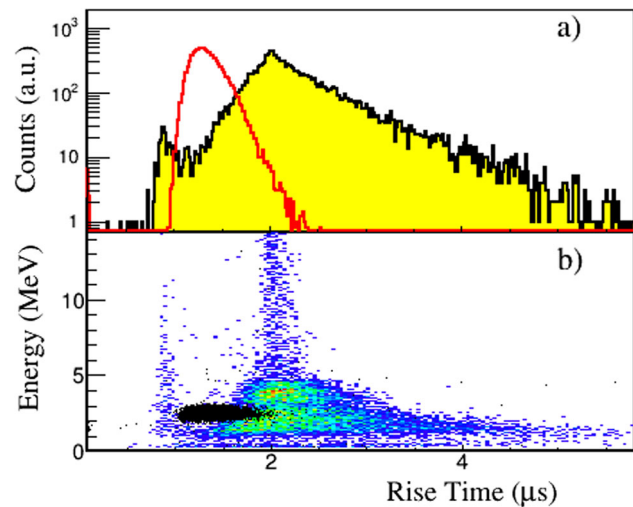


**Fig. 5 a** Rise time spectrum measured for the run with the AmBe source (filled yellow histogram) and with the mixed nuclei alpha source (red histogram). **b** The colored plot is the Rise time as a function of the detected energy for the AmBe run. Black dots refer to events collected with the mixed nuclei alpha source



The discrimination between noise and waveforms carrying information relies on the following technique (typical for zero suppression algorithms). The comparison of the difference between the average value of the signal taken in two regions, one before the start of the signal and one in the middle of the digitized range, with a given threshold, close to zero, allows the discrimination. This can be better understood looking again at Fig. 3, showing a typical noise waveform (cyan filled histogram) and a real one (green filled histogram). The gates 1 and 2 in this figure show the regions used to calculate the difference. Figure 4 shows the noise integral evaluated performing the difference between the average value of the signal in the baseline window (gate1) and around the middle of time range of the signal (gate2). A cut in the region of  $\approx$  channel 20 allows to exclude background noise events. Information about the type of the particle can be obtained from the measurement of the rise time 30–80%. Figure 5a, shows the rise-time spectra from the AmBe source (yellow filled histogram) and from a mixed nuclei alpha source (red histogram), constituted by a mixture of the three transuranic elements  $^{239}\text{Pu}$  (5.155 MeV),  $^{241}\text{Am}$  (5.486 MeV),  $^{244}\text{Cm}$  (5.805 MeV). The peak in the yellow histogram at  $\approx 2\mu\text{s}$  is due to signals generated mainly by  $\gamma$ -rays. The alpha peak (red histogram) is well resolved, having the maximum at  $1.3\mu\text{s}$ . However the tails of the distributions are large; this can be better seen in Fig. 5b displaying the energy vs rise time for the detected radiations. The black dots refer to the alpha source. It is evident that the presence of background noise affects the discrimination at low energy. A better discrimination at low energy is instead obtained using the standard Fast–Slow technique, as described in Ref. [13]. More in detail, the Fast value is integrated in the first 600 ns of the digitized signal, while the Slow component is obtained averaging the digitized signal from 900 ns to  $6\mu\text{s}$ . Alternatively, the correlation of Energy and Slow component can be used to discriminate particles, as shown in Fig. 6 where alpha particles from triple mixed source and  $\gamma$ -rays from AmBe source are well discriminated. The choice to plot the energy instead of the fast component is related to a more linear behavior of the former at high energy. This plot shows that  $\gamma$ -rays are resolved with respect to alpha particles even at low energy. In the figure, pile-up events of two alpha particles (with approximately two times the energy of the alpha source) can be observed. The events in the line with the highest ratio between Energy and Slow signals corresponds to events with a rise time of the order of  $1\mu\text{s}$  observed in all measurements with and without sources. These relatively fast signals, see also Fig. 5, could be heavy fragments generated by cosmic rays interactions [21] or more simply muons detected in the photodiode.

**Fig. 6** Energy-Slow plot obtained summing events from an AmBe source and the triple peaks mixed alpha source

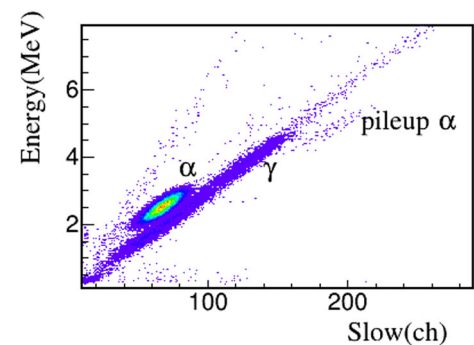


**Fig. 7** Energy spectra of the  $\gamma$ -ray sources used for the detector calibration. AmBe (yellow filled),  $^{60}\text{Co}$  (blue filled),  $^{137}\text{Cs}$  (green filled). Some Gaussian fits of the peaks are also shown as red lines. The energy calibration function and calibration points are plotted in the inset

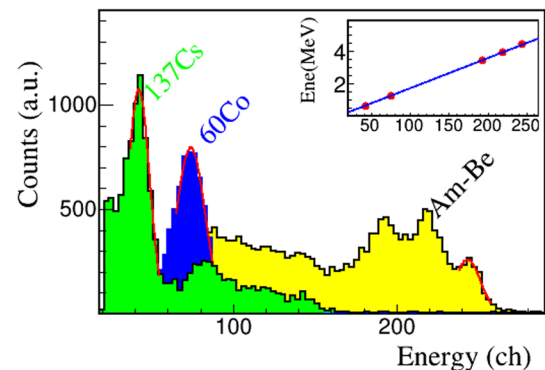
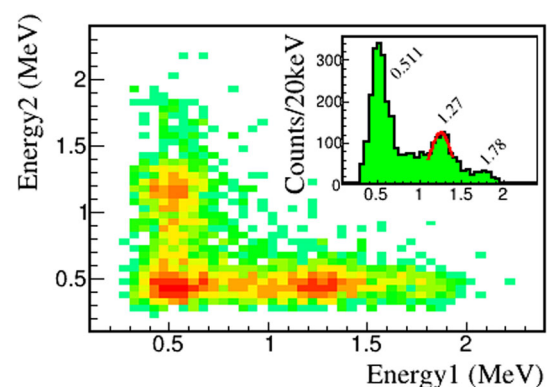


**Fig. 8** Coincidences measurements from the  $^{22}\text{Na}$  source. The peaks relative to coincidences from the two annihilation  $\gamma$ -rays and the main 1.27 MeV  $\gamma$ -ray can be observed. In the inset the energy spectrum of one of the two scintillators is shown, in red the Gaussian fit of the 1.27 MeV peak



#### 4 Measurement with sources

The performance of the CsI(Tl) of the FARCOS telescopes with different radioactive sources has been probed. In addition to the already mentioned AmBe source,  $^{60}\text{Co}$  and  $^{137}\text{Cs}$  sources were employed. Figure 7 shows the spectra obtained with these different sources. As already observed, in the case of the AmBe (yellow filled histogram) the energy resolution is good enough to well resolve full energy, first and second escape peaks. The measured resolution value in the case of the full energy peak is of the order of 140 keV rms, about 3.5%. Unfortunately, the energy resolution is not enough to resolve the two peaks at 1.17 MeV and 1.33 MeV of  $^{60}\text{Co}$  (blue filled histogram); for this reason an average value was used for the calibration. The sigma value of the  $^{137}\text{Cs}$  peak (filled green histogram)  $E_\gamma = 662$  keV is about 123 keV (18%). The inset shows the energy vs channel correlation obtained with the different sources. The small value of the intercept at zero energy—which in case of digital acquisition is expected to be zero—witnesses the good quality of the calibration. The deviation from zero can be attributed to the presence of small non-linear contributions present at very low energy in the scintillators. The reliability of the calibration has been further checked using 511 keV and 1.27 MeV  $\gamma$ -rays from  $^{22}\text{Na}$  together with peaks of  $^{40}\text{K}$  and  $^{208}\text{Tl}$  radioactive elements present in the environment.

The test with the  $^{22}\text{Na}$  source was performed requiring the coincidence between the two 511 keV  $\gamma$ -rays, coming from the  $e^+$  annihilation, or the coincidence between one of such low energy  $\gamma$ -rays and the 1.27 MeV  $\gamma$ -ray emitted by the source. For this measurement the source was placed between two FARCOS telescopes, thus with a detection solid angle of about  $4\pi$ . Figure 8 shows the coincidence matrix between the energy of the  $\gamma$ -rays detected in the two detectors. The expected coincidence events are visible in the plot. Coincidence events between one 511 keV  $\gamma$ -ray and the pile-up between the other 511 keV and the 1.27 MeV  $\gamma$ -ray are

**Fig. 9** Energy spectra collected with triple mixed alpha source (blue),  $^{22}\text{Na}$   $\gamma$ -ray source (pink) and AmBe  $\gamma$ -rays source (yellow)

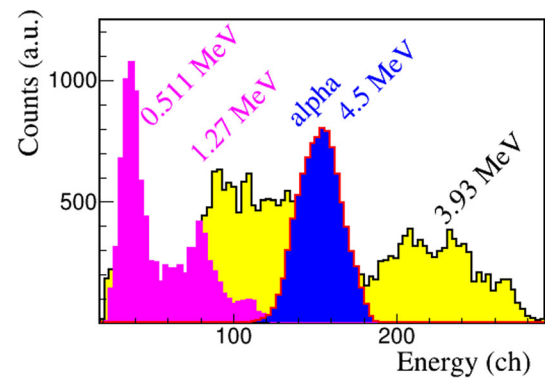
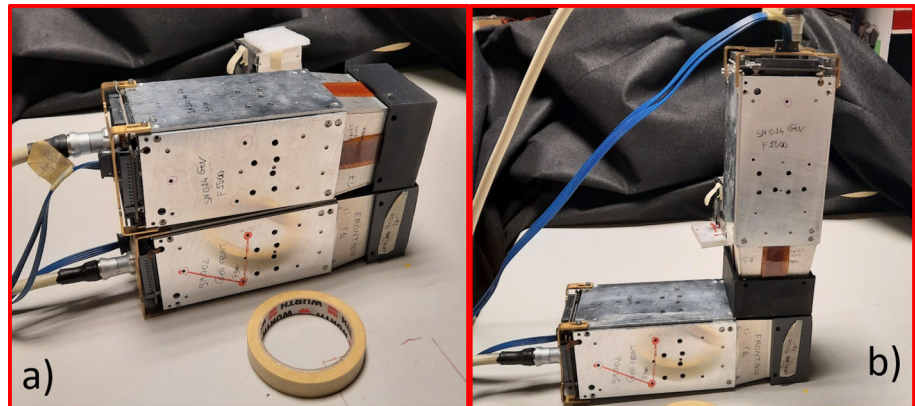


**Fig. 10 a** Picture of two FARCOS telescopes mounted one over the other for the measurement of cosmic rays traveling across the scintillators along the horizontal side. **b** For the measurement of cosmic rays impinging on a scintillator along its length one of the telescopes was placed in vertical position over the other



also present at 1.78 MeV. The inset of Fig. 8 shows the energy spectrum observed in one of the two detectors. The energy resolution, derived from the Gaussian fits is respectively 100 keV rms and 124 keV for the 0.511 MeV and for the 1.27 MeV, while the deviation from the linear fit is of the order of 10 keV.

The energy resolution seems rather poor, but we emphasize that the gain of the whole system was adjusted to be able to detect high energy protons up to 100 MeV. The light yield of CsI(Tl) detectors is one of the largest in the case of inorganic scintillators, however is rather low in absolute value, producing several tens of photons per one keV of gamma energy [22]. Considering the specifications of the used electronics, the  $^{137}\text{Cs}$  signal used for the calibration is around 7 mV, higher than the corresponding measured noise, which is around 1 mV.

The response of the CsI(Tl) to alpha particles has been studied irradiating the same detector with the triple mixed alpha source as previously mentioned in the text. The source was placed in air at about 5 mm from the surface of the detector. The three peaks cannot be distinguished at the current resolution. Taking into account the energy loss in air and in the Mylar foil in front of the detector (2  $\mu\text{m}$ ), an average alpha particle energy of 4.5 MeV can be expected. Figure 9 shows the measured alpha peak superimposed on the uncalibrated histogram of the inset of Fig. 8. The quenching [23, 24] in the response function of the CsI(Tl) scintillator to alpha particles is evident also by the comparison with the yellow AmBe energy spectrum. The energy response to alpha particle is about 30% smaller than the one to  $\gamma$ -rays.

## 5 Measurement with cosmic rays and environmental radioactivity

Due to the size of the detectors, the efficiency to cosmic rays is small. Long runs, from 1 to 4 days, were used to measure the cosmic rays traveling through the scintillators, both horizontally and vertically placed (i.e. with an absorption length of 3.2 cm or 6 cm respectively), as shown in Fig. 10. Coincidences between detectors placed in the same vertical plane were required to select cosmic rays impinging in vertical direction. Figure 11 shows the resulting spectra relative to setup shown in the Fig. 10a (green) and relative to set-up shown in the Fig. 10b (yellow). The inset shows the inclusive spectrum corresponding to the detector placed in vertical position (cyan), together with the spectrum obtained in coincidence with the underlying detector (yellow). The maximum of energy loss for muons impinging in the vertical direction and thus having the full absorption length of 6 cm, is 35.1 MeV, corresponding to a loss of  $\approx 5.8$  MeV/cm. The obtained value depends on the average energy muon spectrum at the laboratory site and on the attenuation factor due to the possible presence of concrete in the roof. This is compatible with a GEANT4 simulation considering a coverage of 0.2 m thick concrete.

**Fig. 11** Cosmic rays detected along the vertical (filled yellow) and horizontal (filled green) absorption length of one detector. The inset shows the inclusive detected energy spectrum of the detector in vertical position (filled cyan) and the spectrum obtained in coincidence with the underlying detector (filled yellow)

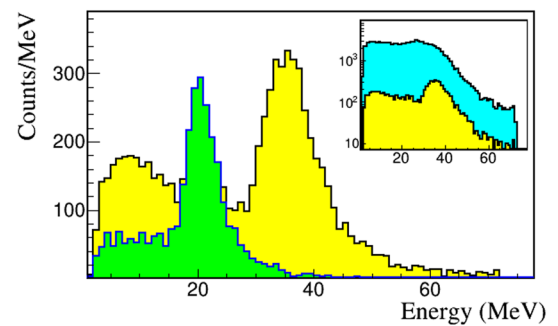
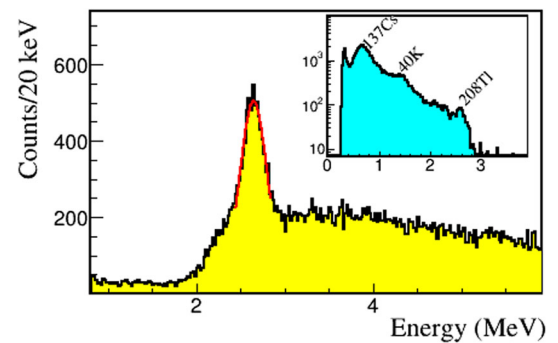


**Fig. 12**  $^{208}\text{Tl}$  spectrum detected during the run with cosmic rays using 2 MeV energy threshold. In the inset the background was measured with lower threshold evidencing the  $^{40}\text{K}$  and  $^{137}\text{Cs}$  natural background emission



Similar results within an error of 0.1 MeV have been obtained in the horizontal configuration (Fig. 10a), despite the analysis is more difficult due the truncated pyramid shape of the scintillators. Outcomes are in agreement with similar measurements performed with simple parallepiped shaped detectors [25].

The run of 4 days performed in the vertical configuration, applying a threshold of 2 MeV in order to save disk space, highlighted the presence of a peak at 2.6 MeV, as shown in Fig. 12. This peak can be attributed to the decay of  $^{208}\text{Tl}$ . This nucleus is populated in the decay chain of  $^{232}\text{Th}$  [26]. It has a life time of  $\approx 3$  minutes and decays  $\beta$  to  $^{208}\text{Pb}$ . Being the spin parity of  $^{208}\text{Tl}$   $5^+$  and the  $Q$ -value of the transition nearly 5 MeV, many  $^{208}\text{Pb}$  excited levels, with large spin are populated. Most of such high spin levels cannot decay directly to the ground state. They decay mostly through the  $3^-$  2.6 MeV level of  $^{208}\text{Pb}$ . The observed peak is therefore populated by the  $\gamma$ -rays emitted from this decay. The sensitivity of the detector can be deduced by the integral of the peak, about 3800 counts (background subtracted) corresponding to a rate of  $\approx 40$  counts/h. Lowering the energy threshold, peaks of  $^{40}\text{K}$  and  $^{137}\text{Cs}$  of the natural radioactivity background can be observed as shown in the inset energy spectrum of Fig. 12. In this histogram the  $^{208}\text{Tl}$  high energy peak can be still noted even if it has a much smaller intensity with respect to the other decays.

## 6 Conclusions and outlook

The response of the CsI(Tl) scintillators of FARCOS telescopes has been analysed using standard  $\gamma$ -ray sources, cosmic rays and the environmental background. Notwithstanding the relatively low gain of the preamplifiers designed to match the dynamics of high energy particles, low energy  $\gamma$ -rays of 511 keV due to  $e^+$  annihilation have been measured. This feature allows the use of the FARCOS array not only as a charged particles correlator, i.e. what it was designed for, but also for the measurement of the  $\gamma$ -ray decay of excited states. This could be useful, for the study of radioactive nuclei, expected to be populated in reactions that will be performed at INFN-LNS (Laboratori Nazionali del Sud dell'INFN) with the new FRAISE fragment separator [27–31], soon available. The obtained energy resolution is not comparable to that obtained with germanium detectors. However, this can be high enough when defined channels are selected. Moreover, requiring the presence of particles in coincidence makes it possible to select information about spin and parity of these levels.

Furthermore, experiments like the search for the  $\gamma$ -ray decay of high energy level of  $^{12}\text{C}$ , recently performed with the CHIMERA detector [1], and in particular the state-of-the-art search of a possible Efimov state on this nucleus [32, 33] could be performed with improved precision due to the gain in resolution of FARCOS scintillators as compared to the CHIMERA CsI(Tl).

The extremely good quality of the developed ASIC preamplifier could pave the way to the construction of a simplified version of the FARCOS detector consisting just of only one or two CsI(Tl) detectors. The low power consumption of the ASIC preamplifier could help to prepare a portable detection system with good efficiency in the measurement of environmental radioactivity for the monitoring of dangerous sites. In addition, the ability to detect in coincidence annihilation  $\gamma$ -rays could be used for the identification of contaminants  $\beta^+$  emitter. Work is in progress also in this direction.

**Acknowledgements** This work has been partially funded by the DGAPA-UNAM IG101423 and CONACYT 315839 Grants, by the “Programma ricerca di Ateneo UNICT 2020-22 linea 2”, and by European Union - (NextGeneration EU), through MUR-PNRR Project SAMOTHRACE (ECS00000022).

**Funding** Open access funding provided by Università degli Studi di Catania within the CRUI-CARE Agreement.

**Data Availability Statement** This manuscript has associated data in a data repository. [Authors’ comments: Data sets generated during the current study will be made available on reasonable request.]

**Open Access** This article is licensed under a Creative Commons Attribution 4.0 International License, which permits use, sharing, adaptation, distribution and reproduction in any medium or format, as long as you give appropriate credit to the original author(s) and the source, provide a link to the Creative Commons licence, and indicate if changes were made. The images or other third party material in this article are included in the article’s Creative Commons licence, unless indicated otherwise in a credit line to the material. If material is not included in the article’s Creative Commons licence and your intended use is not permitted by statutory regulation or exceeds the permitted use, you will need to obtain permission directly from the copyright holder. To view a copy of this licence, visit <http://creativecommons.org/licenses/by/4.0/>.

## References

1. A. Pagano et al., Fragmentation studies with the CHIMERA detector at LNS in Catania: recent progress. *Nucl. Phys. A* **734**, 504–511 (2004). <https://doi.org/10.1016/j.nuclphysa.2004.01.093>
2. M. Pârlog, B. Borderie, M. Rivet, G. Tbcaru, A. Chbihi, M. Elouardi, N. Le Neindre, O. Lopez, E. Plagnol, L. Tassan-Got, G. Auger, C. Bacri, N. Bellaize, F. Bocage, R. Bougault, B. Bouriquet, R. Brou, P. Buchet, J. Charvet, J. Colin, D. Cussol, R. Dayras, A. Demeyer, D. Doré, D. Durand, J. Frankland, E. Galichet, E. Genouin-Duhamel, E. Gerlic, S. Hudan, D. Guinet, P. Loutesse, F. Lavaud, J. Laville, J. Lecolley, C. Leduc, R. Legrain, M. Louvel, A. Maskay, L. Nalpas, J. Normand, J. Péter, E. Rosato, F. Saint-Laurent, J. Steckmeyer, B. Tamain, O. Tirel, E. Vient, C. Volant, J. Wieleczko, Response of CsI(Tl) scintillators over a large range in energy and atomic number of ions. Part II: calibration and identification in the INDRRA array. *Nucl. Instrum. Methods Phys. Res. Sect. A Accel. Spectrom. Detect. Assoc. Equip.* **482**(3), 693–706 (2002). [https://doi.org/10.1016/S0168-9002\(01\)01712-0](https://doi.org/10.1016/S0168-9002(01)01712-0)
3. R. De Souza, N. Carlin, Y. Kim, J. Ottarson, L. Phair, D. Bowman, C. Gelbke, W. Gong, W. Lynch, R. Pelak, T. Peterson, G. Poggi, M. Tsang, H. Xu, The MSU Miniball  $4\pi$  fragment detection array. *Nucl. Instrum. Methods Phys. Res. Sect. A Accel. Spectrom. Detect. Assoc. Equip.* **295**(1), 109–122 (1990). [https://doi.org/10.1016/0168-9002\(90\)90429-A](https://doi.org/10.1016/0168-9002(90)90429-A)
4. Z. Ying Wei, R. Yuan Zhu, A study on undoped CsI crystals. *Nucl. Instrum. Methods Phys. Res. Sect. A Accel. Spectrom. Detect. Assoc. Equip.* **326**(3), 508–512 (1993). [https://doi.org/10.1016/0168-9002\(93\)90852-9](https://doi.org/10.1016/0168-9002(93)90852-9)
5. N. Atanov, V. Baranov, L. Borrel, C. Bloise, J. Budagov, S. Ceravolo, F. Cervelli, F. Colao, M. Cordelli, G. Corradi, Y. Davydov, S.D. Falco, E. Diociaiuti, S. Donati, B. Echenard, C. Ferrari, A. Gioiosa, S. Giovannella, V. Giusti, V. Glagolev, F. Grancagnolo, D. Hampai, F. Happacher, D. Hitlin, M. Martini, S. Middleton, S. Miscetti, L. Morescalchi, D. Paesani, D. Pasciuto, E. Pedreschi, F. Porter, F. Raffaelli, A. Saputi, I. Sarra, F. Spinella, A. Taffara, A.M. Zanetti, R.Y. Zhu, The Mu2e crystal calorimeter: an overview. *Instruments* **6**(4), 60 (2022). <https://doi.org/10.3390/instruments6040060>
6. W. Skulski, M. Momayezi, Particle identification in CsI(Tl) using digital pulse shape analysis. *Nucl. Instrum. Methods Phys. Res. Sect. A Accel. Spectrom. Detect. Assoc. Equip.* **458**(3), 759–771 (2001). [https://doi.org/10.1016/S0168-9002\(00\)00938-4](https://doi.org/10.1016/S0168-9002(00)00938-4)
7. F. Amorini et al., Investigation of the dependence of CsI(Tl) scintillation time constants and intensities on particle’s energy, charge and mass through direct fitting of digitized waveforms. *IEEE Trans. Nucl. Sci.* **59**(4), 1772–1780 (2012). <https://doi.org/10.1109/TNS.2012.2201499>
8. O. Lopez, M. Pârlog, B. Borderie, M. Rivet, G. Lehaut, G. Tabacaru, L. Tassan-got, P. Pawłowski, E. Bonnet, R. Bougault, A. Chbihi, D. Dell’Aquila, J. Frankland, E. Galichet, D. Gruyer, M. La Commara, N. Le Neindre, I. Lombardo, L. Manduci, P. Marini, J. Steckmeyer, G. Verde, E. Vient, J. Wieleczko, Improving isotopic identification with INDRRA Silicon-CsI(Tl) telescopes. *Nucl. Instrum. Methods Phys. Res. Sect. A Accel. Spectrom. Detect. Assoc. Equip.* **884**, 140–149 (2018). <https://doi.org/10.1016/j.nima.2017.12.041>
9. E. Fioretto, F. Innocenti, G. Viesti, M. Cinausero, L. Zuin, D. Fabris, M. Lunardon, G. Nebbia, G. Prete, CsI(Tl)-photodiode detectors for  $\gamma$ -ray spectroscopy. *Nucl. Instrum. Methods Phys. Res. Sect. A Accel. Spectrom. Detect. Assoc. Equip.* **442**(1), 412–416 (2000). [https://doi.org/10.1016/S0168-9002\(99\)01264-4](https://doi.org/10.1016/S0168-9002(99)01264-4)
10. L. Meng, D. Ramsden, V. Chirkin, V. Potapov, O. Ivanov, S. Ignatov, The design and performance of a large-volume spherical CsI(Tl) scintillation counter for gamma-ray spectroscopy. *Nucl. Instrum. Methods Phys. Res. Sect. A Accel. Spectrom. Detect. Assoc. Equip.* **485**(3), 468–476 (2002). [https://doi.org/10.1016/S0168-9002\(01\)02107-6](https://doi.org/10.1016/S0168-9002(01)02107-6)
11. G. Cardella et al., Particle gamma correlations in  $^{12}\text{C}$  measured with the CsI(Tl) based detector array CHIMERA. *Nucl. Instrum. Methods Phys. Res. Sect. A Accel. Spectrom. Detect. Assoc. Equip.* **799**, 64–69 (2015). <https://doi.org/10.1016/j.nima.2015.07.054>
12. M. Alderighi et al., Particle identification method in the CsI(Tl) scintillator used for the CHIMERA  $4\pi$  detector. *Nucl. Instrum. Methods Phys. Res. Sect. A Accel. Spectrom. Detect. Assoc. Equip.* **489**(1), 257–265 (2002). [https://doi.org/10.1016/S0168-9002\(02\)00800-8](https://doi.org/10.1016/S0168-9002(02)00800-8)
13. L. Acosta et al., Probing the merits of different event parameters for the identification of light charged particles in CHIMERA CsI(Tl) detectors with digital pulse shape analysis. *IEEE Trans. Nucl. Sci.* **60**(1), 284–292 (2013). <https://doi.org/10.1109/TNS.2013.2237789>
14. A. Badalà, M.L. Cognata, R. Nania et al., Trends in particle and nuclei identification techniques in nuclear physics experiments. *La Rivista del Nuovo Cimento* **45**, 189–276 (2022). <https://doi.org/10.1007/s40766-021-00028-5>
15. L. Acosta, et al., The FARCOS detection system: the first application in a real experiment. 2019 IEEE Nuclear Science Symposium and Medical Imaging Conference (NSS/MIC) pp. 1–4 (2019). <https://doi.org/10.1109/NSS/MIC42101.2019.9060013>
16. E. De Filippo, et al., The FARCOS array at LNS. in preparation (2023)
17. A. Castoldi, C. Guazzoni, T. Parsani, A CMOS frontend for scintillators readout by photodiodes for nuclear physics experiments. *IEEE Trans. Nucl. Sci.* **64**(10), 2678–2682 (2017). <https://doi.org/10.1109/TNS.2017.2741962>
18. E. Pollacco, G. Grinyer, F. Abu-Nimeh, T. Ahn, S. Anvar, A. Arokjaraj, Y. Ayyad, H. Baba, M. Babo, P. Baron, D. Bazin, S. Beceiro-Novo, C. Belkhiria, M. Blaizot, B. Blank, J. Bradt, G. Cardella, L. Carpenter, S. Ceruti, E. De Filippo, E. Delagnes, S. De Luca, H. De Witte, F. Druillolle, B. Duclous, F. Favella, A. Fritsch, J. Giovaninazzo, C. Gueye, T. Isobe, P. Hellmuth, C. Huss, B. Lachacinski, A. Laffoley, G. Lebertre, L. Legard, W. Lynch, T. Marchi, L. Martina, C. Maugeais, W. Mittig, L. Nalpas, E. Pagano, J. Pancin, O. Polshchuk, J. Pedroza, J. Pibernat, S. Primault, R. Raabe, B. Raine, A. Rebbi, M. Renaud, T. Roger, P. Roussel-Chomaz, P. Russotto, G. Saccà, F. Saillant, P. Sizun, D. Suzuki, J. Swartz, A. Tizon, A. Trifiró, N. Usher, G. Wittwer, J. Yang, GET: a generic electronics system for TPCs and nuclear physics instrumentation. *Nucl. Instrum. Methods Phys. Res. Sect. A Accel. Spectrom. Detect. Assoc. Equip.* **887**, 81–93 (2018). <https://doi.org/10.1016/j.nima.2018.01.020>



19. V.T. Jordanov, G.F. Knoll, Digital synthesis of pulse shapes in real time for high resolution radiation spectroscopy. *Nucl. Instrum. Methods Phys. Res. Sect. A Accel. Spectrom. Detect. Assoc. Equip.* **345**(2), 337–345 (1994). [https://doi.org/10.1016/0168-9002\(94\)91011-1](https://doi.org/10.1016/0168-9002(94)91011-1)
20. F. Risitano, et al., FARCOS response test in stability and temperature. LNS report 2020 pp. 73–74 (2021). <https://www.lns.infn.it/it/download/download-history/category/35-Ins-activity-report.html>
21. S. Abe, S. Asami, M. Eizuka, S. Futagi, A. Gando, Y. Gando, T. Gima, A. Goto, T. Hachiya, K. Hata, K. Hosokawa, K. Ichimura, S. Ieki, H. Ikeda, K. Inoue, K. Ishidoshiro, Y. Kamei, N. Kawada, Y. Kishimoto, M. Koga, M. Kurasawa, T. Mitsui, H. Miyake, T. Nakahata, K. Nakamura, R. Nakamura, H. Ozaki, T. Sakai, I. Shimizu, J. Shirai, K. Shiraishi, A. Suzuki, Y. Suzuki, A. Takeuchi, K. Tamae, H. Watanabe, Y. Yoshida, S. Obara, A.K. Ichikawa, S. Yoshida, S. Umehara, K. Fushimi, K. Kotera, Y. Urano, B.E. Berger, B.K. Fujikawa, J.G. Learned, J. Maricic, S.N. Axani, Z. Fu, J. Smolksy, L.A. Winslow, Y. Efremenko, H.J. Karwowski, D.M. Markoff, W. Tornow, S. Dell’Oro, T. O’Donnell, J.A. Detwiler, S. Enomoto, M.P. Decowski, K.M. Weerman, C. Grant, A. Li, H. Song, Measurement of cosmic-ray muon spallation products in a xenon-loaded liquid scintillator with KamLAND. *Phys. Rev. C* **107**, 054612 (2023). <https://doi.org/10.1103/PhysRevC.107.054612>
22. J. de Haas, P. Dorenbos, C. van Eijk, Measuring the absolute light yield of scintillators. *Nucl. Instrum. Methods Phys. Res. Sect. A Accel. Spectrom. Detect. Assoc. Equip.* **537**(1), 97–100 (2005). <https://doi.org/10.1016/j.nima.2004.07.243>. (Proceedings of the 7th International Conference on Inorganic Scintillators and their Use in Scientific and Industrial Applications)
23. E. Valtonen, J. Peltonen, J.J. Torsti, Response of BGO and CsI(Tl) scintillators to heavy ions. *Nucl. Instrum. Methods Phys. Res. Sect. A Accel. Spectrom. Detect. Assoc. Equip.* **286**(1), 169–174 (1990). [https://doi.org/10.1016/0168-9002\(90\)90219-V](https://doi.org/10.1016/0168-9002(90)90219-V)
24. N. Colonna, G. Wozniak, A. Veeck, W. Skulski, G. Goth, L. Manduci, P. Milazzo, P. Mastinu, Calibration of the response function of CsI(Tl) scintillators to intermediate-energy heavy ions. *Nucl. Instrum. Methods Phys. Res. Sect. A Accel. Spectrom. Detect. Assoc. Equip.* **321**(3), 529–534 (1992). [https://doi.org/10.1016/0168-9002\(92\)90063-A](https://doi.org/10.1016/0168-9002(92)90063-A)
25. G. Cardella, et al., Energy loss of cosmic rays in the CHIMERA-FARCOS CsI(Tl) detectors. LNS report 2021-22 p. in print (2023). <https://www.lns.infn.it/it/download/download-history/category/35-Ins-activity-report.html>
26. G.G. Kulikov, A.N. Shmelev, V.A. Apse, E.G. Kulikov, Proliferation protection of uranium due to the presence of U-232 decay products as intense sources of hard gamma radiation. *Nucl. Energy Technol.* **8**(2), 121–126 (2022). <https://doi.org/10.3897/nucet.8.87814>
27. P. Russotto, L. Calabretta, G. Cardella, G. Cosentino, E.D. Filippo, B. Gnoffo, M.L. Cognata, N. Martorana, E. Pagano, R. Pizzone, L. Quattrocchi, S. Romano, A. Russo, D. Santonocito, Status and perspectives of the INFN-LNS in-flight fragment separator. *J. Phys. Conf. Ser.* **1014**(1), 12016 (2018). <https://doi.org/10.1088/1742-6596/1014/1/012016>
28. A. Russo et al., Preliminary design of the new FRAGMENT In-flight SEPARATOR (FRAISE). *Nucl. Instrum. Methods Phys. Res. Sect. A Accel. Spectrom. Detect. Assoc. Equip.* **463**, 418–420 (2020). <https://doi.org/10.1016/j.nimb.2019.04.037>
29. N. Martorana, Status of the FraLSe facility and diagnostics system. *Il Nuovo Cimento* **44**(C), 1 (2021). <https://doi.org/10.1393/ncc/i2021-21001-2>
30. N. Martorana et al., The new fragment in-flight separator at INFN-LNS. *Il Nuovo Cimento* **45**(C), 63 (2022). <https://doi.org/10.1393/ncc/i2022-22063-2>
31. N.S. Martorana, G. Cardella, C. Guazzoni, E.V. Pagano, A.D. Russo, P. Russotto, L. Acosta, A. Amato, L. Calabretta, A. Caruso, S. Cavallaro, L. Cosentino, M. Costa, E. De Filippo, G. De Luca, E. Geraci, B. Gnoffo, C. Maiolino, S. Passarello, S. Pirrone, G. Politi, S. Pulvirenti, F. Risitano, F. Rizzo, D. Santonocito, A. Trifiró, M. Trimarchi, S. Tudisco, G. Vecchio, Radioactive ion beam opportunities at the new FRAISE facility of INFN-LNS. *Front. Phys.* **10**, 1058419 (2022). <https://doi.org/10.3389/fphy.2022.1058419>
32. V. Efimov, Energy levels arising from resonant two-body forces in a three-body system. *Phys. Lett. B* **33**(8), 563–564 (1970). [https://doi.org/10.1016/0370-2693\(70\)90349-7](https://doi.org/10.1016/0370-2693(70)90349-7)
33. G. Cardella, A. Bonasera, N. Martorana et al., Search for rare 3- $\alpha$  decays in the region of the Hoyle state of  $^{12}\text{C}$ . *Nucl. Phys. A* **1020**, 122395 (2022). <https://doi.org/10.1016/j.nuclphysa.2022.122395>